C. HUET, D. BOURGOIN, S. RICHEMOND. Rhéologie des matériaux anisotropes. *Rheology of anisotropic materials* CR 19e Coll. GFR, Paris, Nov. 1984, Editions CEPADUES, Toulouse, 1986, pp. 79-92

Elastic-wave surfaces in anisotropic media

Surfaces d'ondes élastiques dans des milieux anisotropes

R.D. KRIZ, H.M. LEDBETTER

Materials Research Engineer and Metallurgist Center for Materials Science
National Bureau of Standards
Boulder, Colorado U.S.A. 80303

RÉSUMÉ

A l'aide des solutions de l'équation de Christoffel, certaines particularités topologiques intéressantes de surfaces d'ondes sont décrites pour des milieux anisotropes. Ces particularités comprennent des intersections surface transversale-surface longitudinale et une conversion continue mode transversal-mode longitudinal sur une meme surface. Pour la symétrie orthorhombique (mmm), des intersections surface transversale-surface transversale se produisent pour tous les cristaux: les surfaces transversales s'interconnectent et forment une seule surface. De plus, certains cristaux orthorhombiques présentent une intersection surface longitudinale-surface transversale telle que les trois surfaces s'interconnectent pour former une seule surface. Une intersection surface longitudinale-surface transversale signifie qu'une vitesse d'onde transversale sera supérieure à une vitesse d'onde longitudinale. Une conversion mode longitudinal-mode transversal signifie que les deux modes, longitudinal et transversal, co-existent sur la meme surface. Plusieurs cas réels sont considérés, y compris le bois et un matériau composite renforcé de fibres.

ABSTRACT

Based on Christoffel-equation solutions, some interesting wave-surface topological features are described for anisotropic media. These features include crossovers of transverse-longitudinal surfaces and continuous transverse-longitudinal mode conversion over a single surface. For orthorhombic symmetry (mmm), crossovers of transverse-transverse surfaces occur for all known cases: the transverse surfaces interconnect and form a single surface. Beyond this, some orthorhombic crystals exhibit a longitudinal-transverse crossover that causes all three surfaces to interconnect into a single surface. Crossover of longitudinal and transverse surfaces means that a transverse wave velocity will exceed a longitudinal wave velocity. A longitudinal-transverse mode conversion means that both longitudinal and transverse modes exist on the same wave surface. We consider several real cases, including wood and reinforced composites.

1 - INTRODUCTION

Representation of solid-state physical properties by geometric surfaces has obvious utility, as described by Nye [1]. For high symmetry materials, Nye [2] and Lekhnitskii [3] describe the construction of elastic-constant representation surfaces. For lower-symmetry cases the increased complexity of the elastic-constant tensor prevents simple representations. The present study focuses on the motion of stress-wave deformation fields in anisotropic materials and, especially, their graphical representation. We find several peculiarities of velocity surfaces and deformation fields. These peculiarities relate to relationships among components of the elastic-stiffness tensor.

Stress-wave deformation fields in anisotropic media can be approximated by plane-wave solutions to the elastic-wave equation. This simplification leads to Christoffel equations [4]:

$$(C_{ijk\ell}\ \nu_j\nu_k - \rho v^2\delta_{i\ell})\ p_\ell = 0, \tag{1}$$

where $C_{ijk\ell}$ is the fourth-rank elastic-stiffness tensor, ν_i are direction cosines of the wave vector (normal to the plane wave) relative to the material axes, X_i, ρ is the mass density, v is the phase velocity of the plane wave parallel to ν_i, and $\delta_{i\ell}$ is the Kronecker delta. Equation (1) represents an eigenvalue problem with three eignvalues, ρv^2, and three eigenvectors that correspond to particle-displacement direction cosines (or polarizations), p_ℓ. The orientation of the particle displacement with respect to the wave vector is denoted by subscripts (t, qt, qℓ) on phase velocities: t means p_i is transverse to ν_i ($p_i\nu_i = 0$), qt (quasi-transverse) means the largest component of p_i is transverse to ν_i ($0 < \nu_i p_i < 1/\sqrt{2}$), and q$\ell$ (quasi-longitudinal) means the largest component of p_i is parallel to ν_i ($1/\sqrt{2} < \nu_i p_i < 1$). Along principal material axes, pure transverse waves and pure longitudinal waves must exist for all wave velocities.

From eq. (1) we can draw the phase-velocity surface (eigenvalues) and displacement field (eigenvectors) by considering all possible propagation directions (wave vectors). Both Musgrave [5] and Auld [6] used this method to study the influence of a material's elastic symmetry on the wave-surface geometries. Recently, Musgrave [7] described new wave-surface geometries where all surfaces interconnect into a single-surface for spruce wood. Independently, Ledbetter and Kriz [8] explained how peculiar mode transitions in the deformation field relate to this single surface geometry for a calcium-formate crystal. In both studies the unique wave-surface geometries relate to inequalities among elastic-stiffness tensor components. Studies by Al'shits and Lothe [9] also show a special case where no degeneracy occurs for a hypothetical orthorhombic material and a single surface cannot exist. In the present study we summarize these elastic-topological peculiarities for both crystalline and fiber-reinforced materials. When examined from the viewpoint of wave propagation, physically realizable combinations of these peculiarities lead to remarkable deformation fields.

The propagation direction of moving displacement fields in anisotropic media is also influenced by peculiarities in elastic anisotropy. Using Huygens's principle, Musgrave [5] demonstrated graphically how the propagation direction can deviate from the wave vector. This direction is called the energy-flux vector,

$$E_j = -C_{ijk\ell}\ u_{k,\ell}\dot{u}_i \tag{2}$$

where u_i is the displacement vector for a plane wave,

$$u_i = Ap_i\cos\nu(vt-\nu_i X_i/\nu) \tag{3}$$

where t is time and $\nu = (\nu_i\nu_i)^{1/2}$. The velocity of propagation in the direction of E_i is called the group velocity, v_g. For isotropic materials E_i and v_g coincide with ν_i and v. For anisotropic materials, E_i deviates from ν_i by

an angle, $\Delta = \cos^{-1} v_i L_i$, where L_i are the direction cosines of E_i. For plane homogeneous waves Hayes and Musgrave [10] show that the same deviation angle, Δ, exists between v_g and v.

For hexagonal-symmetry fiber-reinforced materials, we demonstrate the influence of fiber volume fraction on the propagation direction and mode transitions. We also consider fiber-reinforced materials such as wood, which has orthorhombic symmetry.

2 - ANALYSIS

2.1 - Wave surfaces and displacement fields

For materials with orthorhombic elastic symmetry, the 21 independent elastic stiffnesses, $C_{ijk\ell}$, reduce to nine that can be written as a 6x6 symmetrical matrix using Voigt's notation,

$$C_{ij} = \begin{vmatrix} C_{11} & C_{12} & C_{13} & 0 & 0 & 0 \\ & C_{22} & C_{23} & 0 & 0 & 0 \\ & & C_{33} & 0 & 0 & 0 \\ & & & C_{44} & 0 & 0 \\ & & & & C_{55} & 0 \\ & & & & & C_{66} \end{vmatrix} \qquad (4)$$

The characteristic equation of the eigenvalue problem defined in eq. (1) becomes for orthorhombic symmetry, the symmetrical determinant.

$$\begin{vmatrix} (C_{11}\nu_1^2 + C_{66}\nu_2^2 + C_{55}\nu_3^2) - \rho v^2 & (C_{12} + C_{66})\nu_1\nu_2 & (C_{13} + C_{55})\nu_3\nu_1 \\ & (C_{66}\nu_1^2 + C_{22}\nu_2^2 + C_{44}\nu_3^2) - \rho v^2 & (C_{23} + C_{44})\nu_2\nu_3 \\ & & (C_{55}\nu_1^2 + C_{44}\nu_2^2 + C_{33}\nu_3^2) - \rho v^2 \end{vmatrix} = 0 \qquad (5)$$

For all possible orientations of the wave vector ν_i, the roots of eq. (5) can be graphed as three unique phase-velocity surfaces. It is convenient to examine the intersections of these surfaces with the three principal orthogonal planes. Relationships describing the phase-velocity surfaces in each plane can be derived from (5). Reference [6] gives

$\underline{X_1 - X_2 \text{ plane}}$: $v_t = [(C_{44}n + C_{55}m)/\rho]^{1/2}$ (6)

$$v_{q\ell},\ v_{qt} = \{[C_{66} + C_{11}m + C_{22}n \pm \sqrt{(C_{66} + C_{11}m + C_{22}n)^2 - 4C}]/2\rho\}^{1/2} \qquad (7,8)$$

where $C = (C_{11}m + C_{66}n)(C_{66}m + C_{22}n) - (C_{12} + C_{66})^2 mn$, where $m = \cos^2\theta$ and $n = \sin^2\theta$. The angle θ is measured positively from X_i to X_j such that $i < j$. Similarly for the other two planes,

$\underline{X_1 - X_3 \text{ plane}}$: $v_t = [(C_{44}n + C_{66}m)/\rho]^{1/2}$ (9)

$$v_{q\ell},\ v_{qt} = \{[C_{55} + C_{11}m + C_{33}n \pm \sqrt{(C_{55} + C_{11}m + C_{33}n)^2 - 4C'}]/2\rho\}^{1/2} \qquad (10,11)$$

where $C' = (C_{11}m + C_{55}n)(C_{55}m + C_{33}n) - (C_{13} + C_{55})^2 mn$;

X_2-X_3 plane: $$v_t = [(C_{66}m + C_{55}n)/\rho]^{1/2} \quad (12)$$

$$v_{q\ell},\ v_{qt} = \{[C_{44} + C_{22}m + C_{33}n \pm \sqrt{(C_{44} + C_{22}m + C_{33}n)^2 - 4C']/2\rho\}^{1/2} \quad (13,14)$$

where $C' = (C_{22}m + C_{44}n)(C_{44}m + C_{33}n) - (C_{23} + C_{44})^2 mn$.

For hexagonal materials with the unique axis X_3, the velocity surface is axially symmetric. Thus, solutions are calculated as functions of $+\theta$ from X_3:

$$v_t(\theta) = [(C_{44}m + C_{66}n)/\rho]^{1/2} \quad (15)$$

$$v_{qt}(\theta),\ v_{q\ell}(\theta) = [(C_{44} + C_{11}n + C_{33}m \mp \sqrt{C})/2\rho]^{1/2} \quad (16, 17)$$

where $C = [(C_{11}-C_{44})n + (C_{44} - C_{33})m]^2 + (C_{13} + C_{44})^2 \sin^2 2\theta$.

One should note that subscripts (t, qt, qℓ) assigned to the wave velocities are only labels. In special cases, displacement polarizations t, qt, qℓ, and ℓ may coexist on the same velocity surface [8]. Thus, rarely, eqs. (7, 8, 10, 11, 13, 14, 16, 17) yield polarizations different from the designated qt, qℓ subscripts. Equations (6, 9, 12, 15) represent exceptions where v_t is always a pure-transverse wave for all orientations.

Because of algebraic complexity, eigenvector solutions of eq. (1) for orthorhombic materials were calculated numerically by backsubstituting ρv^2 into eq. (1). For hexagonal symmetries, eigenvector solutions of eq. (1) are much simpler and are written here as the ratio $P_1:P_2:P_3$.

$$P_1 = [\nu_1^2(C_{11} + C_{12})/2]^{1/2}/[\rho v^2 - (C_{11} - C_{12})/2 - C_{44}\nu_3^2] \quad (18)$$

$$P_2 = [\nu_2^2(C_{11} + C_{12})/2]^{1/2}/[\rho v^2 + (\nu_2^2 - \nu_1^2)C_{11}/2 + C_{12}/2 - \nu_3^2 C_{44}] \quad (19)$$

$$P_3 = [2\nu_3^2(C_{23} + C_{44})/(C_{11} + C_{12})]^{1/2} / \{\rho v^2 + (\nu_2^2 - \nu_1^2)C_{44} + \nu_3^2[2(C_{23} + C_{44})^2/(C_{11} + C_{12}) - C_{33}]\} \quad (20)$$

2.2 - Propagation directions

The angular deviation between the propagation direction (energy-flux vector) and the wave vector is calculated by

$$\Delta = \cos^{-1}\nu_i L_i \quad (21)$$

where L_i are the direction cosines of E_i. Kriz and Stinchcomb [11] calculated L_i for orthorhombic materials. For materials with hexagonal symmetry, Kriz and Ledbetter [12] calculated L_i for transformations in the X_2-X_3 plane ($\nu_1 = 0$):

$$L_1 = C_{66}p_1p_2\nu_2 + C_{44}p_1p_3\nu_3 \quad (22)$$

$$L_2 = C_{66}p_1^2\nu_2 + C_{22}p_2^2\nu_2 + C_{23}p_2p_3\nu_3 + C_{44}(p_2p_3\nu_3 + p_3^2\nu_2) \quad (23)$$

$$L_3 = C_{22}p_3^2\nu_3 + C_{33}p_2p_3\nu_2 + C_{44}(p_1^2\nu_3 + p_2p_3\nu_2) \quad (24)$$

For fiber-reinforced materials we studied the influence of fiber volume fraction on the properties listed above. This is accomplished by calculating effective C_{ij} from relationships derived by Datta, Ledbetter, and Kriz [13].

3 - RESULTS AND DISCUSSION

For elastically isotropic solids, the phase-velocity surfaces are concentric spheres where t and qt surfaces coincide (see Fig. 1). All waves are pure mode. Mechanical stability requires that v_ℓ exceed $v_t\sqrt{4/3}$. Thus, the ℓ and

surfaces cannot intersect for isotropic media.

For anistropic materials, e.g. calcium formate, wave surfaces can intersect. The most common intersection occurs for the t and qt surfaces; Figs. 2 and 3 exemplify this type of intersection.

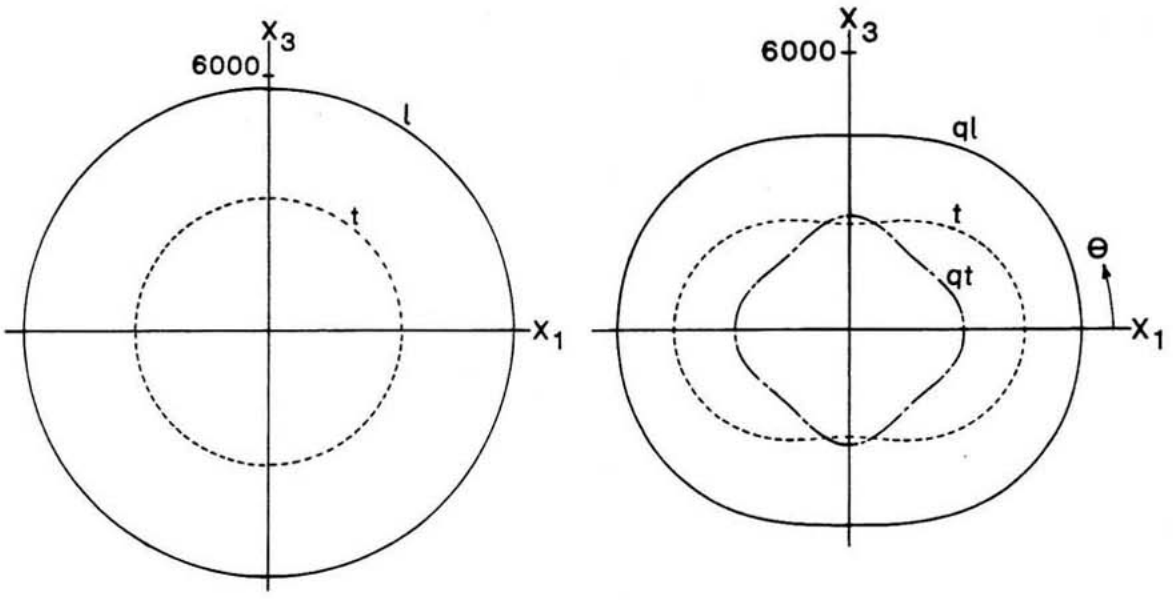

Fig. 1. Polar diagram of phase velocity (m/s) for a typical isotropic material: polycrystalline 304 stainless steel. Elastic constants [14] are C_{11} = 261, C_{12} = 106 GPa; ρ = 7.88 g/cm^3.

Fig. 2. Polar diagram of phase velocity (m/s) in the X_1-X_3 plane of a material that exhibits t-qt intersections: calcium formate [$Ca(HCOO)_2$], which is orthorhombic. Elastic constants [15] are C_{11} = 49.2, C_{22} = 24.4, C_{33} = 35.4, C_{12} = 24.8, C_{13} = 24.5, C_{23} = 14.5, C_{44} = 10.5, C_{55} = 12.1, C_{66} = 28.2 GPa; ρ = 2.02 g/cm^3.

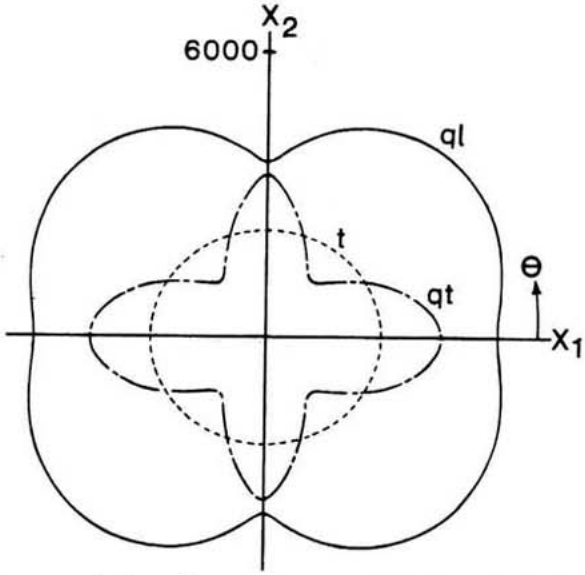

Fig. 3. Same as Fig. 2, except for X_1-X_2 plane, which exhibits t-qt intersections in each quadrant. See also Fig. 5.

Less common is an intersection of a ql surface with a qt or t surface; Fig. 4 shows such an example. Thus, for this one case, in one direction $v_{q\ell} = v_t$; and along X_2 (and near X_2) v_t actually exceeds $v_{q\ell}$. In the X_1-X_2 plane for this

same material no intersection occurs but a polarization-mode transition occurs. Figure 5 illustrates this mode transition; it shows polarization vectors at 9° increments as double-headed arrows. To more clearly understand the relationship between surface intersections and mode transitions, Ledbetter and Kriz [8] drew an isometric combination of principal planes shown in Figs. 2-4. Figure 6 shows this isometric diagram.

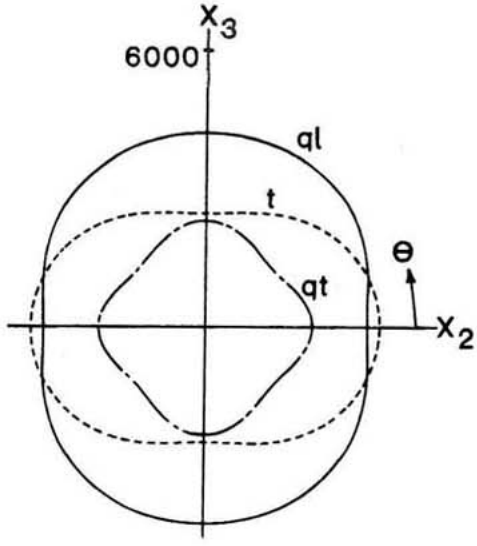

Fig. 4. Same as Fig. 2, except for X_2-X_3 plane, which exhibits t-qℓ intersections in each quadrant.

From Fig. 6 we observe that for calcium formate all surfaces interconnect into a single surface. Close examination of eqs. (6-14) reveals that necessary and sufficient conditions for this geometry are

$$C_{11} > C_{33} > C_{66} > C_{22} > C_{55} > C_{44} \tag{25}$$

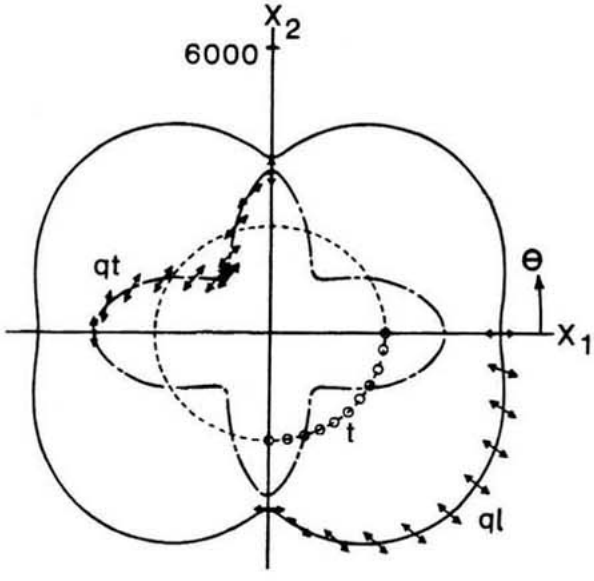

Fig. 5. Same as Fig. 3, but with polarization (particle displacement) vector indicated by arrows. Fastest wave is pure longitudinal along X_1, but pure transverse along X_2. Second wave is pure transverse along X_1, but pure longitudinal along X_2, where $v_{q\ell}$ becomes a transverse wave and exceeds a longitudinal wave speed. Third wave is pure transverse for all directions.

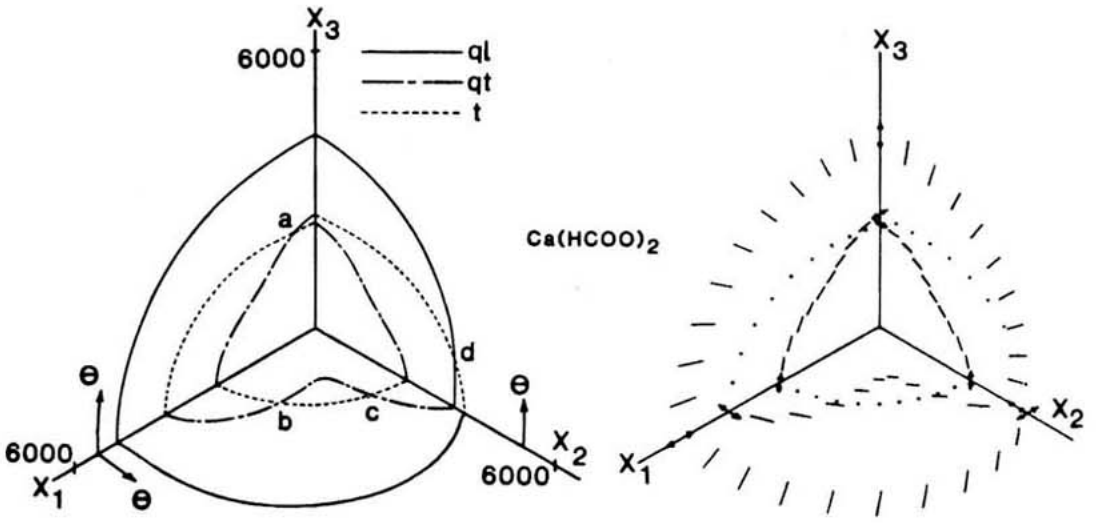

Fig. 6. (a) Isometric plot of phase-velocity (m/s) surfaces intersecting the three principal orthogonal planes: calcium formate; see Figs. 2, 3, and 4. This figure summarizes the qt-t intersections at a, b, and c, and the t-qℓ intersection at d. Together, these topological features reduce the usual three velocity surfaces to a single surface. (b) Isometric plot of displacement fields coincident with phase-velocity surfaces of the same material. Line segments represent displacement direction contained within orthogonal planes. Dots represent displacements normal to orthogonal planes. Arrows represent pure modes. Mode transitions occur only in the X_1-X_2 plane.

Closer examination of other inequalities leads to several geometries [8]. From these studies we concluded that, except for calcium formate, all reported orthorhombic cases require interconnection of the qt and t surfaces into a single surface (see Fig. 7).

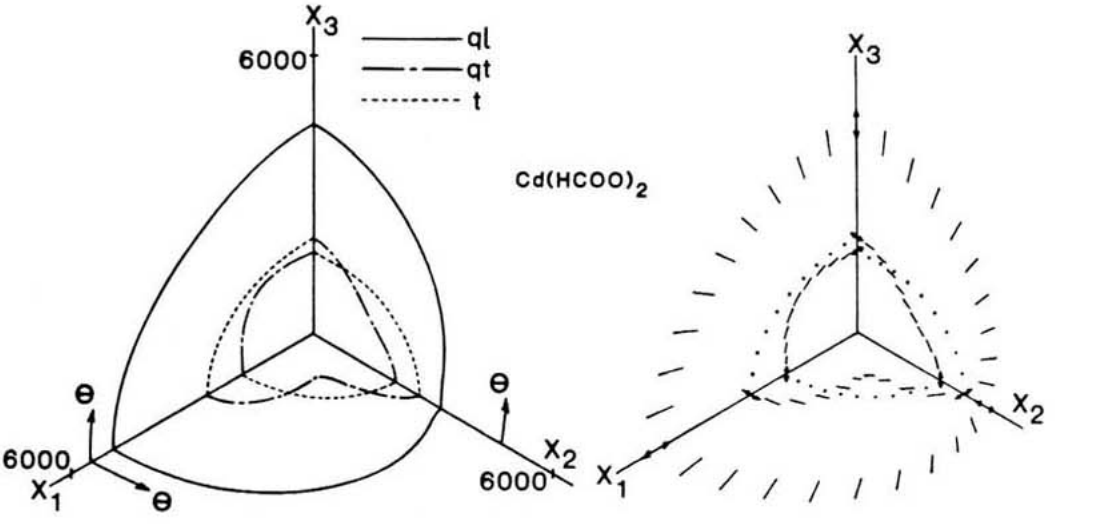

Fig. 7. (a) Isometric plot of phase-velocity (m/s) surfaces intersecting the three principal orthogonal planes: cadmium formate [$Cd(HCOO)_2$], which is orthorhombic. Elastic constants [15] are C_{11} = 50.0, C_{22} = 20.5, C_{33} = 41.1, C_{12} = 24.6, C_{13} = 27.3, C_{23} = 16.4, C_{44} = 8.53, C_{55} = 6.32, C_{66} = 14.1 GPa; ρ = 2.02 g/cm^3. (C_{11}, C_{22}, C_{33}) > (C_{44}, C_{55}, C_{66}). (b) Isometric plot of displacement fields coincident with phase-velocity surfaces of the same material. Graphical conventions are same as Fig. 6(b). There are no mode transitions. Two additional geometries shown in Figs. 8 and 9 are also possible but, as yet, no examples are known.

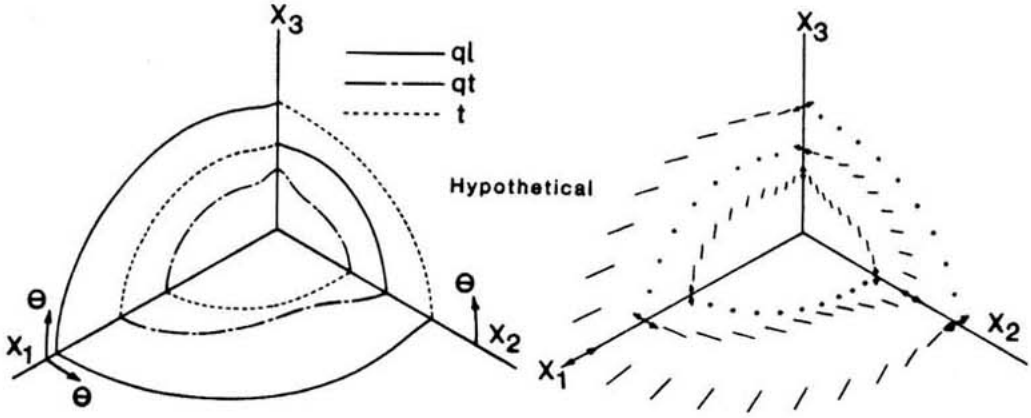

Fig. 8. (a) Isometric plot of phase-velocity surfaces intersecting the three principal orthogonal planes of a hypothetical orthorhombic material whose elastic constants satisfy the inequalities $C_{11} > C_{66} > C_{55} > C_{22} > C_{44} > C_{33}$. This figure demonstrates three unconnected wave-velocity surfaces. See also Musgrave [7] and Al'shits and Lothe [9]. (b) Isometric plot of displacement fields coincident with phase-velocity surfaces of the same material. Graphical conventions are same as Fig. 6(b). Mode transitions occur in all planes.

Independently, Musgrave [7] used similiar inequalities to classify the various geometries of materials with orthorhombic symmetry. Musgrave observed that spruce wood also satisfies an inequality similar to eq. (25) except $C_{66} > C_{11}$ (see also Fig. 10). Musgrave ex-plained the inequality requirements for surfaces with no intersections (see Fig. 8). These wave surfaces were also studied by Al'shits and Lothe [9]. Later, Holm and Lothe [14] studied the displacement polarization fields for body waves in anisotropic media without an acoustic axis.

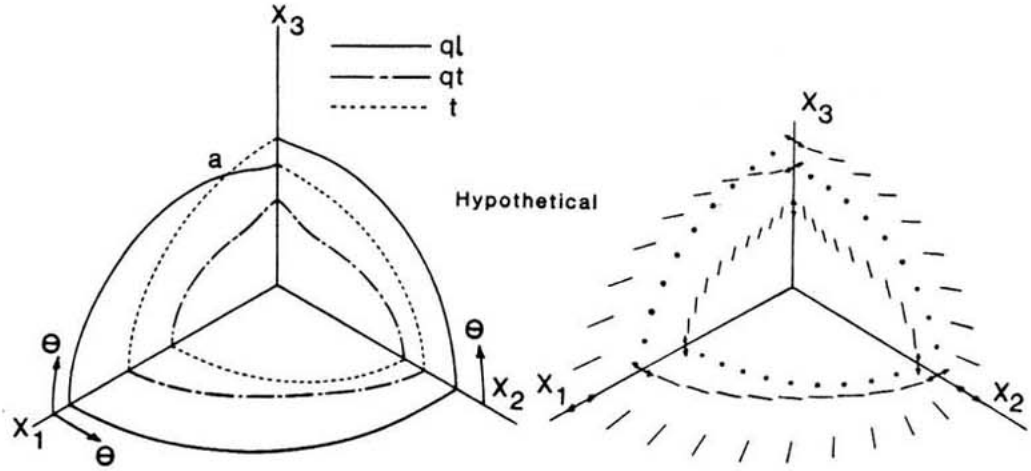

Fig. 9. (a) Isometric plot of phase-velocity surfaces intersecting the three principal orthogonal planes of a hypothetical orthorhombic material whose elastic constants satisfy the inequalities $C_{11} > C_{22} > C_{66} > C_{44} > C_{55} > C_{33}$. This figure demonstrates a qℓ-qt crossover at a. (b) Isometric plot of displacement fields coincident with phase-velocity surfaces of the same material. Graphical conventions are same as in Fig. 6(b). Mode transitions occur only in the X_1-X_3 and X_3-X_2 planes.

From studies of Jaswon and Gillis [17, 18] we observe that the orthorhombic elastic symmetry for spruce wood can be modeled by aligned rectangular cellulose fibers arranged in a rectangular array (see Fig. 11) where the cellulose fibers also have orthorhombic symmetry. With the present model it would be possible to transition between geometries of Fig. 6 and Fig. 7 by changing the ratios a:b and c:d for dimensions shown in Fig. 11. It may also be possible to construct special fiber-array geometries that satisfy conditions for orthorhombic symmetries shown in Figs. 8 and 9, which are presently only hypothetical possibilities.

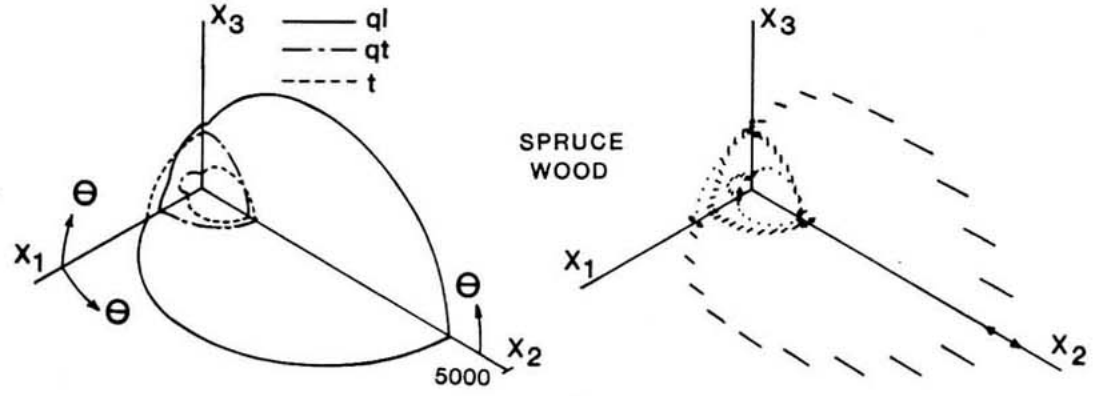

Fig. 10. (a) Isometric plot of phase-velocity (m/s) surfaces intersecting the three principal orthogonal planes for spruce wood, which is orthorhombic [7]. Elastic constants are C_{11} = 0.44, C_{22} = 16.3, C_{33} = 0.78, C_{12} = 0.31, C_{13} = 0.20, C_{23} = 0.43, C_{44} = 0.62, C_{55} = 0.40, C_{66} = 0.77 GPa; ρ = 1 g/cm^3. A single surface exists similar to Fig. 6 except $C_{66} > C_{11}$ hence t-ql occurs in the X_1-X_3 plane. (b) Isometric plot of displacement fields coincident with phase-velocity surfaces of the same material. Graphical conventions are same as in Fig. 6(b). Mode transitions occur only in the X_1-X_2 plane.

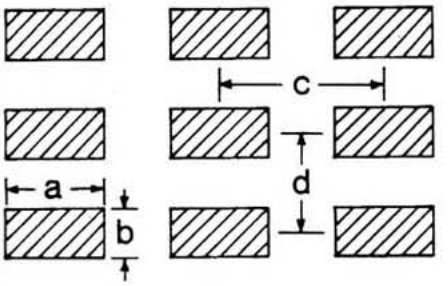

Fig. 11. Cross-section showing morphology of wood after Gillis [18]. Cross-hatched region represents rectangular cellulose fibers surrounded by isotropic matrix.

For aligned fiber-reinforced graphite/epoxy materials with hexagonal symmetry (random array) Kriz and Ledbetter [12] observed several peculiarities in elastic-wave surfaces and displacement fields caused by variations in the fiber volume fraction (see Figs. 12-16). Figures 12 and 13 demonstrate the influence of fiber volume fraction on phase-velocity and group-velocity surfaces. Here we follow Musgrave [5] and plot group velocity as a function of $\theta' = \theta + \Delta$. Large changes in flux-deviation angles, shown in Fig. 15, occur at low fiber volume fractions. Hence, the distorted group-velocity surfaces in Fig. 13 result from these changes in flux-deviation angles with fiber volume fraction.

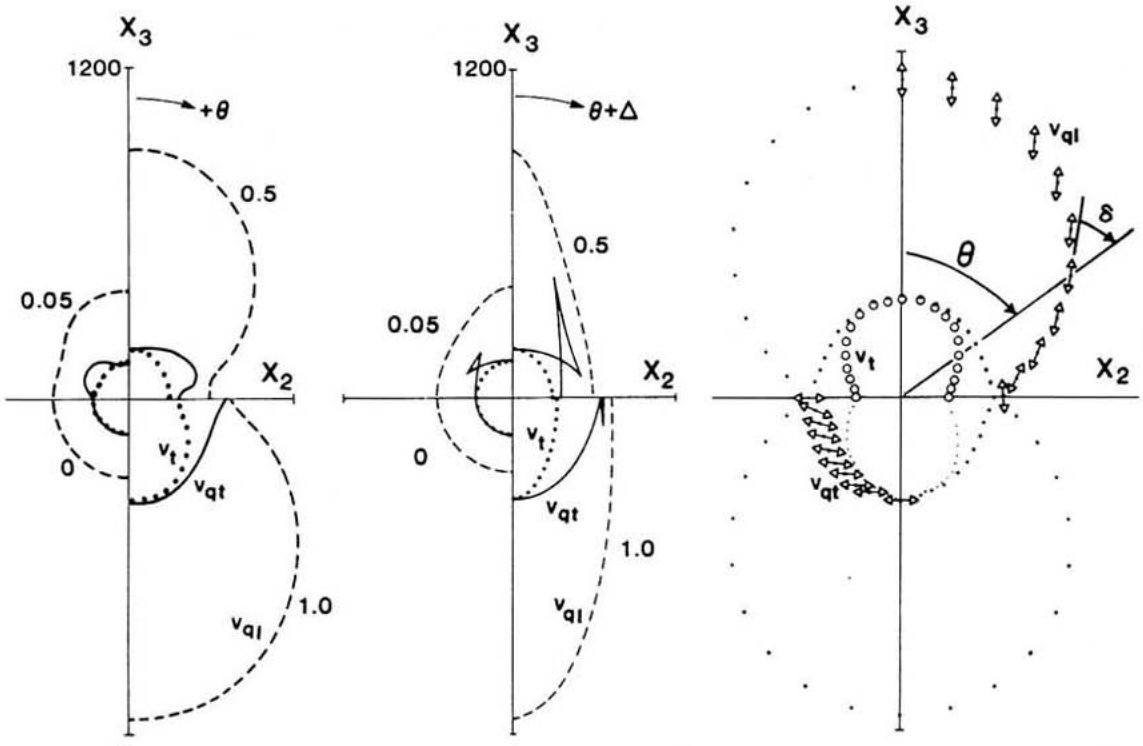

Fig. 12. Phase-velocity (m/s) polar diagram for unidirectional graphite/epoxy at four fiber volume fractions.

Fig. 13. Group-velocity (m/s) polar diagram corresponding to Fig. 12.

Fig. 14. Polar diagram of displacement direction coincident with phase-velocity surfaces at a fiber volume-fraction of 1.0. For clarity, only one quadrant shown.

At a fiber volume fraction of 100% (see Fig. 14) we observed mode transitions similar to calcium formate and spruce wood except that surfaces do not interconnect into a single surface. For the qℓ surface the displacement in the X_2-X_3 plane changes from pure longitudinal along X_3 to pure shear along X_2. Consequently, in the X_1-X_2 plane one observes $v_t > v_\ell$ along X_2 when $C_{44} > C_{22}$.

This mode transition can also be observed in Fig. 16 for various fiber volume fractions. Here the displacement deviations, $\delta = \cos^{-1} v_i p_i$, from the wave vectors are shown versus θ. In Fig. 16 we observe that fiber volume fraction effects a smooth mode transition. The mode transition starts at $V_f = 0.3$ where $v_{q\ell}$ transitions into v_{qt} at $\theta = 56°$. As V_f increases, this mode transition continues predictably; for $V_f > 0.96$, v_{qt} transitions into v_t. Thus, ℓ, qℓ, qt, and t particle displacements are also observed along a single surface for a fiber-reinforced material.

Unlike crystalline materials, variations in propagation directions can occur for fixed orientations in fiber-reinforced materials. Kriz [19] demonstrated how changes in the elastic properties of the matrix component of a unidirectional graphite/epoxy composite can influence the flux deviation angle, Δ. Figure 17 shows the comparison of measurement with theory for the configuration shown in Fig. 18. Here we find that an increase in deviation angle, Δq_t, occurs when absorbed moisture degrades the resin properties. When fiber elastic properties degrade, we predict a decrease in deviation angle, Δ_{qt}. Values of elastic properties are given in [19].

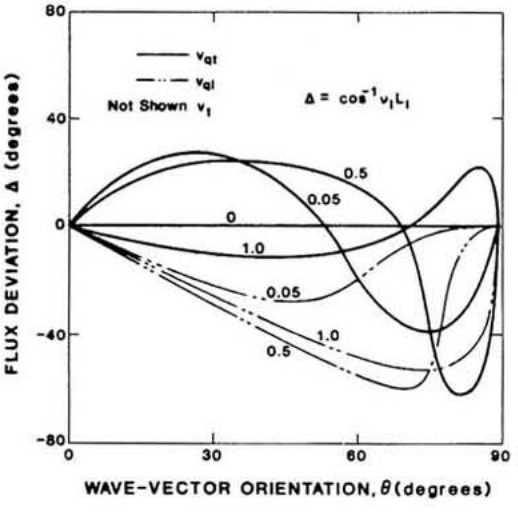

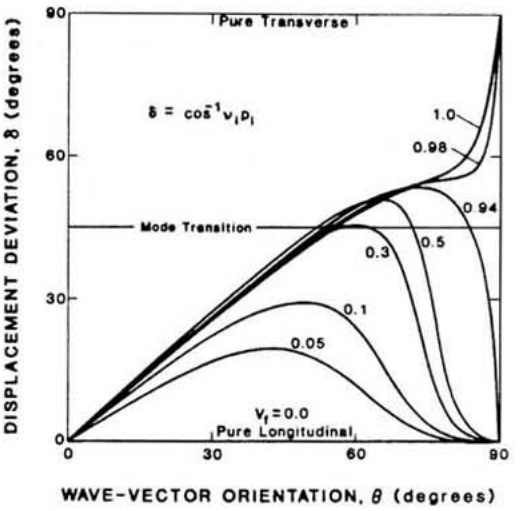

Fig. 15. Flux-deviation angles for various fiber volume-fractions. For clarity, v_t curves are omitted.

Fig. 16. Displacement-direction deviations for $v_{q\ell}$. For higher fiber volume-fractions, a mode transition occurs.

For all materials considered here, we find that all components of the elastic-stiffness tensor satisfy the mechanical-stability conditions (positive-definite strain-energy density).

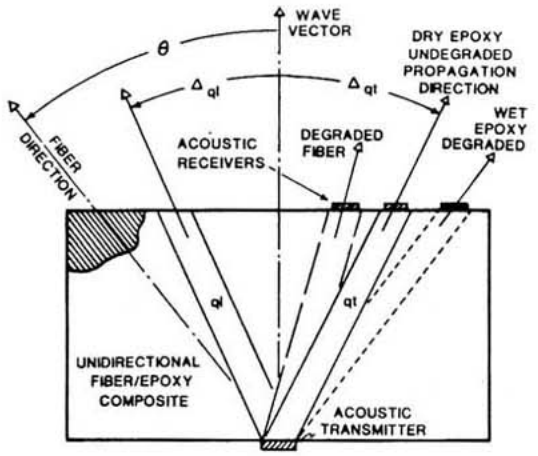

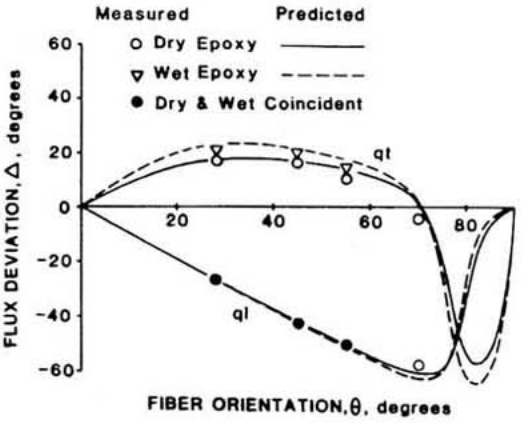

Fig. 17. Schematic diagram of variation in propagation directions in a unidirectional graphite epoxy material.

Fig. 18. Comparison of measured and predicted flux-deviation angles resulting from absorbed moisture degrading only the epoxy elastic properties.

4 - SUMMARY

From previous studies discussed above, for anisotropic media, we find many remarkable topological features of elastic-wave surfaces. For orthorhombic materials we observe that qt and t surfaces must always interconnect into a single surface. Calcium formate and spruce wood are exceptions where qℓ, qt, and t surfaces all interconnect into one surface. These geometries and others are sufficiently defined by inequalities among the diagonal components of the elas-

tic-stiffness tensor. Associated with these geometries we find peculiarities in the displacement fields. For calcium formate and spruce wood we find mode transitions where ℓ, qℓ, qt, and t displacements coexist on the same surface. For fiber-reinforced materials we find that similar mode transitions occur at high fiber volume fractions but interconnections do not result in single surfaces. In both symmetries we observe transverse waves faster than longitudinal waves. For fiber-reinforced materials we also observe a strong influence of fiber volume fraction on propagation direction. For graphite/epoxy we found that variations in propagation direction arise from changes in either fiber or matrix elastic properties.

5 - ACKNOWLEDGMENTS

These studies were supported partly by the Department of Energy, Office of Fusion Energy.

6 - REFERENCES

[1] J. F. Nye, Physical Properties of Crystals, Oxford University Press, London, 1957 (p. 16).

[2] J. F. Nye, Physical Properties of Crystals, Oxford University Press, London, 1957 (p. 143).

[3] S. G. Lekhnitskii, Theory of Elasticity of an Anisotropic Body, Holden-Day, San Francisco, 1963 (p. 15).

[4] M. J. P. Musgrave, Crystal Acoustics, Holden-Day, San Francisco, 1970 (p. 83).

[5] M. J. P. Musgrave, Crystal Acoustics, Holden-Day, San Francisco, 1970 (p. 108).

[6] B. A. Auld, Acoustic Fields and Waves in Solids, Vol.1, Wiley, New York, 1973 (p. 401).

[7] M. J. P. Musgrave, "On an elastodynamic classification of orthorhombic media," Proc. R. Soc. Lond. A374, 401 (1981).

[8] H. M. Ledbetter and R. D. Kriz "Elastic Wave Surfaces in Solids," Phys. Stat. Sol. (b) 114, 475 (1982).

[9] V. I. Al'shits and J. Lothe, "Elastic waves in triclinic crystals II. Topology of polarization fields and some general theorems," Kristallografiya 24, 75 (1979).

[10] M. Hayes and M. J. P. Musgrave, "On Energy Flux Group Velocity," Wave Motion 1, 75 (1979).

[11] R. D. Kriz and W. W. Stinchcomb, "Elastic Moduli of Tranversely Isotropic Fibers and their Composites," Exper. Mech. 19, 41 (1979).

[12] R. D. Kriz and H. M. Ledbetter, "Elastic Representation Surfaces of Unidirectional Graphite/Epoxy Composites in , "Recent Advances in Composites in the United States and Japan, ASTM STP864, J. R. Vinson and M. Taya, Eds., American Society for Testing and Materials, Philadelphia, 1985 (in press).

[13] S. K. Datta, H. M. Ledbetter, and R. D. Kriz, "Calculated Elastic Constants of Composites Containing Anisotropic Fibers," Int. J. Solids Structures 20, 429 (1984).

[14] H. M. Ledbetter and N. V. Frederick and M. W. Austin, "Elastic-constant variability in stainless-steel 304," J. Appl. Phys. 51, 305 (1980).

[15] S. Haussühl, Z. Krist. 118, 33 (1963).

[16] P. Holm and J. Lothe, "The topological nature of the polarization field for body waves in anisotropic elastic media," Proc. R. Soc. Lond. A370, 331 (1980).

[17] M. A. Jaswon, P. P. Gillis, and R. E. Mark, "The elastic constants of crystalline native cellulose," Proc. Roy. Soc. Lond. A306, 389 (1968).

[18] P. P. Gillis, "Elastic moduli for plane stress analyses of unidirectional composites with anisotropic rectangular reinforcement," Fibre Sci. Tech. 2, 193 (170).

[19] R. D. Kriz, "Monitoring Elastic Stiffness Degradation in Graphite/Epoxy Composites," to be published.